Journal of Systems Engineering and Electronics
Vol. 28, No. 3, June 2017, pp.546 – 555

Integrated guidance and control design of the suicide UCAV for terminal attack

Huan Zhou, Hui Zhao, Hanqiao Huang*, and Xin Zhao

Aeronautics and Astronautics Engineering College, Air Force Engineering University, Xi'an 710038, China

Abstract: A novel integrated guidance and control (IGC) design method is proposed to solve problems of low control accuracy for a suicide unmanned combat aerial vehicle (UCAV) in the terminal attack stage. First of all, the IGC system model of the UCAV is built based on the three-channel independent design idea, which reduces the difficulties of designing the controller. Then, IGC control laws are designed using the trajectory linearization control (TLC). A nonlinear disturbance observer (NDO) is introduced to the IGC controller to reject various uncertainties, such as the aerodynamic parameter perturbation and the measurement error interference. The stability of the closed-loop system is proven by using the Lyapunov theorem. The performance of the proposed IGC design method is verified in a terminal attack mission of the suicide UCAV. Finally, simulation results demonstrate the superiority and effectiveness in the aspects of guidance accuracy and system robustness.

Keywords: integrated guidance and control (IGC), unmanned combat aerial vehicle (UCAV), trajectory linearization control (TLC), terminal attack, nonlinear disturbance observer (NDO).

DOI: 10.21629/JSEE.2017.03.14

1. Introduction

The requirement on control accuracy of missiles and suicide unmanned combat aerial vehicles (UCAVs) has become higher and higher in modern complex battlefield [1]. For suicide UCAVs, the terminal mission stage is the most critical and the terminal guidance and control technology is an effective way to improve the attack accuracy.

In the traditional control idea, the guidance subsystem and control subsystem are designed separately. This idea is based on the hypothesis of the frequency spectrum separation of cascade control systems in essence [2 – 4]. In the terminal attack stage of a suicide UCAV, the time constant in the guidance loop is decreasing with the decrease in relative vehicle-target distance, when serious miss distance and fight stability loss of the UCAV occurs [5]. As a result, the performance of the traditional method is constrained.

To deal with this problem, the integrated guidance and control (IGC) is proposed and widely studied [6]. In the IGC design, the guidance system and control system are integrated designed. The deflection commands are calculated and obtained according to the relative movement between the UCAV and target, which can improve the control precision and avoid the stability loss. Since the IGC idea was created by Williams et al. [7] in 1983, large numbers of IGC design methods have become research spots, such as optimal control (OC) [8], backstepping control (BC) [9,10], differential geometry control (DGC) [11], dynamic surface control (DSC) [12], and variable structure control (VSC) [13]. Every method has been proven effective in some aspects, but there are still some shortages: the analytical solution problem of OC, the computation expansion and parameter setting of BC, the modeling error sensitivity of DSC, and the self-buffeting problem of VSC, etc. The trajectory linearization control (TLC) is a novel effective nonlinear tracking and decoupling control method [14], and is increasingly being applied to flight control systems of new missiles and UAVs. Because TLC has the special control structure that the pseudo inverse of matrix is computed in the open loop and the tracking error is adjusted in the closed loop, which makes outputs exponentially stable on the nominal state, so TLC has a certain robustness and anti-interference capacity. In [15], an adaptive neural network technique for nonlinear systems based on TLC was firstly proposed. Reference [16] studied the TLC of actuated underwater vehicles (AUVs) by using the time-scale separation in differential equation singular perturbation theory. Reference [17] put forward a pitching channel IGC design method, because it was only effective in two-dimensional plane, so the application of the method was limited greatly.

Manuscript received January 19, 2016.
*Corresponding author.
This work was supported by the National Natural Science Foundation of China (61601505; 71501184) and the National Aviation Science Foundation of China (20155196022).

In above literature, TLC has been proven effective, but there are still two challenges: the high order and a great deal of uncertainties of the IGC system. Some solution methods are correct theoretically, but they are hard to realize in engineering because of the increasing complexity. Besides, the high order problem is not solved effectively.

The contribution of this paper is developing a novel IGC design method of a suicide UCAV for terminal attack. The reasonable decoupled IGC system model is built based on the three-channel independent design idea, which solves the high order problem of the TLC. Control laws are designed using the TLC, which increases the control accuracy of the suicide UCAV. After that, a nonlinear disturbance observer (NDO) is introduced to estimate and compensate the nonlinear uncertainties, thus guaranteeing the robustness of the controller. Simulation results verify the high precision control performance of the proposed IGC design method and strong robustness in the presence of 20% aerodynamic coefficients uncertainty of both constant and time-varying types.

The rest of this paper is organized as follows: Section 2 builds the IGC system model of the suicide UCAV; Section 3 proposes the IGC design method of the suicide UCAV using the TLC; Section 4 demonstrates the stability of the IGC design method; Section 5 presents the results and discussion. Finally, Section 6 concludes the paper.

2. IGC system model of the suicide UCAV

2.1 Mathematical model of the suicide UCAV

The nonlinear model of the suicide UCAV flight control system [18] is

$$\begin{cases} \dot{\gamma} = \omega_x - \tan\theta(\omega_y \cos\gamma - \omega_z \sin\gamma) \\ \dot{\beta} = \omega_x \sin\alpha + \omega_y \cos\alpha + \dfrac{qSc_z^\beta \beta - P\cos\alpha \sin\beta}{mV} \\ \dot{\alpha} = \tan\beta(-\omega_x \cos\alpha + \omega_y \sin\alpha) + \omega_z - \dfrac{qSc_y^\alpha + P}{mV\cos\beta}\alpha \\ \dot{\omega}_x = \dfrac{qSLm_x^{\delta_x}}{J_x}\delta_x + \dfrac{J_y - J_z}{J_x}\omega_z\omega_y \\ \dot{\omega}_y = \dfrac{qSL}{J_y}(m_y^\beta \beta + m_y^{\delta_y}\delta_y + m_y^{\omega_y}\omega_y) + \dfrac{J_z - J_x}{J_y}\omega_x\omega_z \\ \dot{\omega}_z = \dfrac{qSL}{J_z}(m_z^\alpha \alpha + m_z^{\delta_z}\delta_z + m_z^{\omega_z}\omega_z) + \dfrac{J_y - J_x}{J_z}\omega_y\omega_x \end{cases} \tag{1}$$

where α, β, γ are, respectively, the angles of attack, sideslip and roll; $\omega_z, \omega_y, \omega_x$ are, respectively, the pitching angle rate, yaw angle rate and roll angle rate; $\delta_z, \delta_y, \delta_x$ denote, respectively, the deflection angles of elevator, rudder and aileron; q is the dynamic head; S is the characteristic area; L is the characteristic length; m is the mass of UCAV; J_z, J_y, J_x denote, respectively, the moment of inertia of Z axis, Y axis and X axis; P is the engine trust; V is the velocity; c_y^α, c_z^β denote, respectively, the partial derivative of lift force relative to angle of attack and angle of sideslip; $m_z^{\omega_z}, m_z^\alpha, m_z^{\delta_z}$ represent, respectively, the partial derivative of the dimensionless pitching moment relative to the pitching angle rate, angle of attack and deflection angle of elevator; $m_y^{\omega_y}, m_y^\beta, m_y^{\delta_y}$ represent, respectively, the partial derivative of dimensionless yaw moment relative to the yaw angle rate, angle of yaw and deflection angle of rudder; $m_x^{\delta_x}$ represents the partial derivative of dimensionless roll moment relative to the deflection of aileron.

In order to reduce the difficulties of using the TLC, the nonlinear UCAV model is decoupled based on the three-channel independent design idea. In this idea, the coupling effects with each other are regarded as uncertainties and nonlinear factors with unknown limit. Then, the pitch channel subsystem of the UCAV can be simplified and depicted as

$$\begin{cases} \dot{\alpha} = \omega_z - \dfrac{qSc_y^\alpha + P}{mV}\alpha + \Delta\alpha \\ \dot{\omega}_z = \dfrac{qSL}{J_z}(m_z^\alpha \alpha + m_z^{\delta_z}\delta_z + m_z^{\omega_z}\omega_z) + \Delta\omega_z \end{cases}. \tag{2}$$

The yaw channel subsystem of the UCAV can be simplified and depicted as

$$\begin{cases} \dot{\beta} = \omega_y + \dfrac{qSc_z^\beta - P}{mV}\beta + \Delta\beta \\ \dot{\omega}_y = \dfrac{qSL}{J_y}(m_y^\beta \beta + m_y^{\delta_y}\delta_y + m_y^{\omega_y}\omega_y) + \Delta\omega_y \end{cases}. \tag{3}$$

The roll channel subsystem of the UCAV can be simplified and depicted as

$$\begin{cases} \dot{\gamma} = \omega_x + \Delta\gamma \\ \dot{\omega}_x = \dfrac{qSL}{J_x}m_x^{\delta_x}\delta_x + \Delta\omega_x \end{cases} \tag{4}$$

where $\Delta\alpha, \Delta\beta, \Delta\gamma$ and $\Delta\omega_z, \Delta\omega_y, \Delta\omega_x$ stand for the unknown bounded uncertainties.

2.2 Relative movement between the UCAV and target

In the terminal attack stage, the relative movement between the UCAV and target can be decoupled to two relatively independent motions in the longitudinal and lateral planes. The diagram of relative movement between the UCAV and target in the longitudinal plane and lateral plane is shown in Fig. 1.

In Fig. 1(a), R_y is the relative distance between the UCAV and target, V_{uy}, V_{ty} stand for, respectively, the velocities of the UCAV and target, a_{uy}, a_{ty} stand for, respectively, the accelerations of the UCAV and target, $\varphi_{uy}, \varphi_{ty}$ represent angles between the velocity vector and reference axis, φ_{ry} is the angle of line-of-sight (LOS). All the above quantities are components along the longitudinal plane.

Then, the relative movement equation set of the UCAV and target is obtained as

$$\begin{cases} \dot{R}_y = V_{ty}\cos(\varphi_{ry}-\varphi_{ty}) - V_{uy}\cos(\varphi_{ry}-\varphi_{uy}) \\ R_y\dot{\varphi}_{ry} = -V_{ty}\sin(\varphi_{ry}-\varphi_{ty}) - V_{uy}\sin(\varphi_{ry}-\varphi_{uy}) \end{cases}. \tag{5}$$

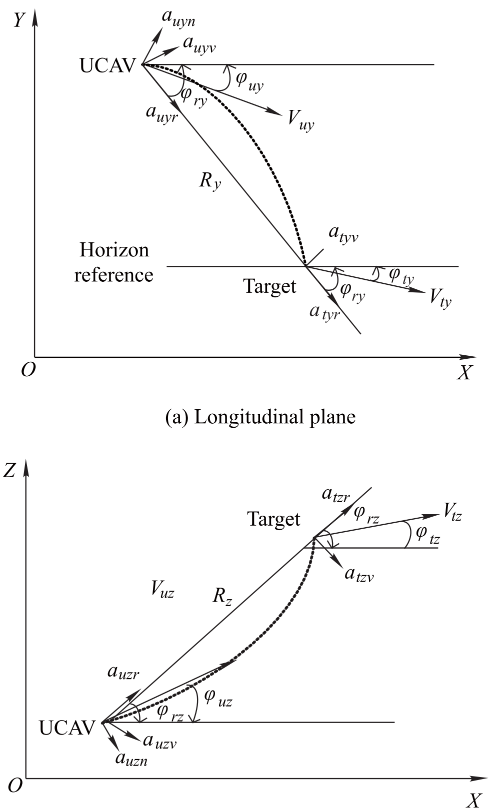

Fig. 1 Diagram of relative movement between the UCAV and target

Let

$$\begin{cases} V_R = \dot{R}_y \\ V_r = R_y\dot{\varphi}_{ry} \end{cases}. \tag{6}$$

Substituting (6) into (5), and taking the derivative of both sides with respect to time, one can obtain

$$\begin{cases} \dot{V}_R = \dfrac{V_r^2}{R_y} + a_{tyr} - a_{uyr} \\ \dot{V}_r = -\dfrac{V_R V_r}{R_y} + a_{tyv} - a_{uyv} \end{cases} \tag{7}$$

with $\dot{V}_R = \ddot{R}_y$, $\dot{V}_r = \dfrac{\mathrm{d}(R_y\dot{\varphi}_{ry})}{\mathrm{d}t}$

$$a_{uyr} = \dot{V}_{uy}\cos(\varphi_{ry}-\varphi_{uy}) + V_{uy}\dot{\varphi}_{uy}\sin(\varphi_{ry}-\varphi_{uy})$$

$$a_{tyr} = \dot{V}_{ty}\cos(\varphi_{ry}-\varphi_{ty}) + V_{ty}\dot{\varphi}_{ty}\sin(\varphi_{ry}-\varphi_{ty})$$

$$a_{uyv} = V_{uy}\dot{\varphi}_{uy}\cos(\varphi_{ry}-\varphi_{uy}) - \dot{V}_{uy}\sin(\varphi_{ry}-\varphi_{uy})$$

$$a_{tyv} = V_{ty}\dot{\varphi}_{ty}\cos(\varphi_{ry}-\varphi_{ty}) - \dot{V}_{ty}\sin(\varphi_{ry}-\varphi_{ty})$$

where a_{uyr}, a_{tyr} are components along the sight directions of a_{uy}, a_{ty}, and a_{uyv}, a_{tyv} are normal components along the sight directions of a_{uy}, a_{ty}.

Substituting (6) into (7), we have

$$\ddot{\varphi}_{ry} = -\frac{2\dot{R}_y}{R_y}\dot{\varphi}_{ry} + \frac{1}{R_y}a_{tyv} - \frac{1}{R_y}a_{uyv}. \tag{8}$$

When the angle between the UCAV velocity vector and LOS is small enough, the equation $a_{uyn} \approx a_{uyv}$ is correct, where a_{uyn} is the normal acceleration of the UCAV. Thus, (8) is approximated by

$$\ddot{\varphi}_{ry} = -\frac{2\dot{R}_y}{R_y}\dot{\varphi}_{ry} - \frac{1}{R_y}a_{uyn} + \Delta\varphi_{ry} \tag{9}$$

where $\Delta\varphi_{ry} = \dfrac{1}{R_y}a_{tyv}$, $a_{uyn} = \dfrac{qSc_y^\alpha + P}{m}\alpha$.

Similarly, for the lateral plane, we have

$$\ddot{\varphi}_{rz} = -\frac{2\dot{R}_z}{R_z}\dot{\varphi}_{rz} + \frac{1}{R_z}a_{uzn} + \Delta\varphi_{rz} \tag{10}$$

where $\Delta\varphi_{rz} = \dfrac{1}{R_z}a_{tzv}$, $a_{uzn} = \dfrac{qSc_z^\beta - P}{m}\beta$.

2.3 IGC system model of the UCAV

From (9) and (2), one can derive the IGC pitch subsystem model of the UCAV as

$$\begin{cases} \dot{\boldsymbol{x}}_1 = \boldsymbol{f}_1(\boldsymbol{x}_1) + \boldsymbol{g}_{11}(\boldsymbol{x}_1)u_1 + \boldsymbol{g}_{12}(\boldsymbol{x}_1)d_1 \\ y_1 = x_{11} \end{cases} \tag{11}$$

where $\boldsymbol{x}_1 = [\dot{\varphi}_{ry}\ \ \alpha\ \ \omega_z]^{\mathrm{T}}$ denotes the subsystem state, $u_1 = \delta_z$ is the input, y_1 is the output, $x_{11} = \dot{\varphi}_{ry}$, and $d_1 \in \mathbf{R}$ represents unknown coefficients uncertain. The matrices $\boldsymbol{f}_1(\boldsymbol{x}_1), \boldsymbol{g}_{11}(\boldsymbol{x}_1)$ and $\boldsymbol{g}_{12}(\boldsymbol{x}_1)$ are

$$\boldsymbol{f}_1(\boldsymbol{x}) = \begin{bmatrix} -\dfrac{2\dot{R}_y}{R_y}\dot{\varphi}_{ry} - \dfrac{qSc_y^\alpha + P}{mR_y}\alpha \\ \omega_z - \dfrac{qSc_y^\alpha + P}{mV}\alpha \\ \dfrac{qSLm_z^{\omega_z}}{J_z v}\omega_z + \dfrac{qSLm_z^\alpha}{J_z}\alpha \end{bmatrix}$$

$$\boldsymbol{g}_{11}(\boldsymbol{x}_1) = \begin{bmatrix} 0 \\ 0 \\ \dfrac{qSLm_z^{\delta_z}}{J_z} \end{bmatrix}$$

$$\boldsymbol{g}_{12}(\boldsymbol{x}_1) = [\ \Delta\varphi_{ry}\quad \Delta\alpha\quad \Delta\omega_z\ ]^{\mathrm{T}}.$$

From (10) and (3), one can derive the IGC yaw subsystem model of the UCAV as

$$\begin{cases} \dot{\boldsymbol{x}}_2 = \boldsymbol{f}_2(\boldsymbol{x}_2) + \boldsymbol{g}_{21}(\boldsymbol{x}_2)u_2 + \boldsymbol{g}_{22}(\boldsymbol{x}_2)d_2 \\ y_2 = x_{21} \end{cases} \tag{12}$$

where $\boldsymbol{x}_2 = [\dot{\varphi}_{rz}\ \beta\ \omega_y]^{\mathrm{T}}$ denotes the subsystem state, $u_2 = \delta_y$ is the input, y_2 is the output, $x_{21} = \dot{\varphi}_{rz}$, and $d_2 \in \mathbf{R}$ represents the unknown coefficients uncertainty. The matrices $\boldsymbol{f}_2(\boldsymbol{x}_2), \boldsymbol{g}_{21}(\boldsymbol{x}_2)$ and $\boldsymbol{g}_{22}(\boldsymbol{x}_2)$ are

$$\boldsymbol{f}_2(\boldsymbol{x}_2) = \begin{bmatrix} -\dfrac{2\dot{R}_z}{R_z}\dot{\varphi}_{rz} + \dfrac{qSc_z^{\beta} - P}{mR_z}\beta \\ \omega_y + \dfrac{qSc_z^{\beta} - P}{mV}\beta \\ \dfrac{qSLm_y^{\omega_y}}{J_y v}\omega_y + \dfrac{qSLm_y^{\beta}}{J_y}\beta \end{bmatrix}$$

$$\boldsymbol{g}_{21}(\boldsymbol{x}_2) = \begin{bmatrix} 0 \\ 0 \\ \dfrac{qSLm_y^{\delta_y}}{J_y} \end{bmatrix}$$

$$\boldsymbol{g}_{22}(\boldsymbol{x}_2) = [\ \Delta\varphi_{rz} \quad \Delta\beta \quad \Delta\omega_y\ ]^{\mathrm{T}}.$$

From (4), one can derive the IGC roll subsystem model of the UCAV as

$$\begin{cases} \dot{\boldsymbol{x}}_3 = \boldsymbol{f}_3(\boldsymbol{x}_3) + \boldsymbol{g}_{31}(\boldsymbol{x}_3)u_3 + \boldsymbol{g}_{32}(\boldsymbol{x}_3)d_3 \\ y_3 = x_{31} \end{cases} \tag{13}$$

where $\boldsymbol{x}_3 = [\gamma\ \omega_x]^{\mathrm{T}}$ denotes the subsystem state, $u_3 = \delta_x$ is the input, y_3 is the output, $x_{31} = \gamma$, and $d_3 \in \mathbf{R}$ represents the unknown coefficients uncertainty. The matrices $\boldsymbol{f}_3(\boldsymbol{x}_3), \boldsymbol{g}_{31}(\boldsymbol{x}_3)$ and $\boldsymbol{g}_{32}(\boldsymbol{x}_3)$ are

$$\boldsymbol{f}_3(\boldsymbol{x}_3) = \begin{bmatrix} \omega_x \\ 0 \end{bmatrix}, \quad \boldsymbol{g}_{31}(\boldsymbol{x}_3) = \begin{bmatrix} 0 \\ \dfrac{qSLm_x^{\delta_x}}{J_x} \end{bmatrix},$$

$$\boldsymbol{g}_{32}(\boldsymbol{x}_3) = [\Delta\gamma\ \Delta\omega_x]^{\mathrm{T}}.$$

The systems in (11) – (13) can be written altogether as

$$\begin{cases} \dot{\boldsymbol{x}} = \boldsymbol{f}(\boldsymbol{x}) + \boldsymbol{g}_1(\boldsymbol{x})\boldsymbol{u} + \boldsymbol{g}_2(\boldsymbol{x})\boldsymbol{d} \\ \boldsymbol{y} = [y_1\ y_2\ y_3]^{\mathrm{T}} \end{cases} \tag{14}$$

where $\boldsymbol{x} = [\boldsymbol{x}_1\ \ \boldsymbol{x}_2\ \ \boldsymbol{x}_3]^{\mathrm{T}}$ denotes the system state, $\boldsymbol{u} = [u_1\ \ u_2\ \ u_3]^{\mathrm{T}}$ is the input, $\boldsymbol{y}$ is the output, $\boldsymbol{d} = [d_1\ \ d_2\ \ d_3] \in \mathbf{R}^3$ represents unknown coefficients uncertainty, $\boldsymbol{f}(\boldsymbol{x}) = [\boldsymbol{f}_1(\boldsymbol{x}_1)\ \ \boldsymbol{f}_2(\boldsymbol{x}_2)\ \ \boldsymbol{f}_3(\boldsymbol{x}_3)]^{\mathrm{T}}$, $\boldsymbol{g}_1(\boldsymbol{x}) = [\boldsymbol{g}_{11}(\boldsymbol{x}_1)\ \ \boldsymbol{g}_{21}(\boldsymbol{x}_2)\ \ \boldsymbol{g}_{31}(\boldsymbol{x}_3)]^{\mathrm{T}}$, and $\boldsymbol{g}_2(\boldsymbol{x}) = [\boldsymbol{g}_{12}(\boldsymbol{x}_1)\ \boldsymbol{g}_{22}(\boldsymbol{x}_2)\ \boldsymbol{g}_{32}(\boldsymbol{x}_3)]^{\mathrm{T}}$.

3. IGC design of the suicide UCAV using the TLC

For the control systems of missiles and suicide UCAVs, the main design objectives are given [6] as follows:

(i) To intercept the maneuvering targets with small miss distance.

(ii) To maintain the change of the angle of roll near zero throughout the engagement.

(iii) To stabilize the states of the missile.

(iv) To be robust with respect to the inevitable uncertainties.

We design IGC control laws using the TLC and introduce an NDO to improve robustness. The structure of the IGC design is illustrated in Fig. 2.

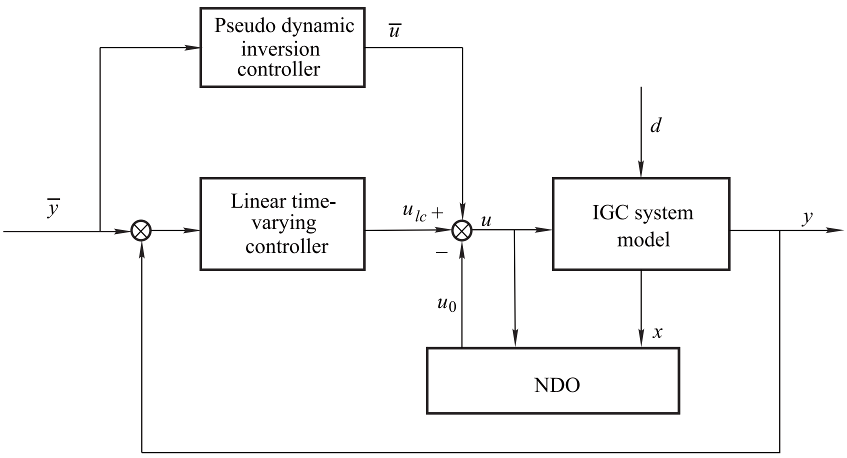

Fig. 2 Structure of the IGC design

3.1 IGC control laws design based on the TLC

For (14), suppose that there exists a nonlinear function $\boldsymbol{g}_0(\boldsymbol{x})$ which can meets the matching condition $\boldsymbol{g}_1(\boldsymbol{x})\boldsymbol{g}_0(\boldsymbol{x}) = \boldsymbol{g}_2(\boldsymbol{x})$.

When $\boldsymbol{d} = \boldsymbol{0}$, define the nominal system state, input and output as $\overline{\boldsymbol{x}}$, $\overline{\boldsymbol{u}}$ and $\overline{\boldsymbol{y}}$, respectively, which satisfy

$$\begin{cases} \dot{\overline{\boldsymbol{x}}} = \boldsymbol{f}(\overline{\boldsymbol{x}}) + \boldsymbol{g}_1(\overline{\boldsymbol{x}})\overline{\boldsymbol{u}} \\ \overline{\boldsymbol{y}} = [\overline{y}_1\ \overline{y}_2\ \overline{y}_3]^{\mathrm{T}} \end{cases}. \tag{15}$$

As $\boldsymbol{g}_1(\overline{\boldsymbol{x}})$ is generalized reversible, we can calculate the nominal input by

$$\overline{\boldsymbol{u}} = \boldsymbol{g}_1^{-1}(\overline{\boldsymbol{x}})[\dot{\overline{\boldsymbol{x}}} - \boldsymbol{f}(\overline{\boldsymbol{x}})]. \tag{16}$$

In order to guarantee the causal relationship of the system, $\dot{\overline{\boldsymbol{x}}}$ will be acquired from the following differentiator:

$$G_{i,diff} = \frac{\omega_{i,diff}s}{s+\omega_{i,diff}}, \quad i = 1, 2. \tag{17}$$

Define the tracking error of the closed loop as $\boldsymbol{e} = \boldsymbol{x} - \overline{\boldsymbol{x}}$ and the controlled variable as $\boldsymbol{u}_{lc} = \boldsymbol{u} - \overline{\boldsymbol{u}}$. Then, the differential equation of dynamic characteristic of $\boldsymbol{e}$ is

$$\begin{gathered}\dot{\boldsymbol{e}} = \dot{\boldsymbol{x}} - \dot{\overline{\boldsymbol{x}}} = \\ \boldsymbol{f}(\overline{\boldsymbol{x}}+\boldsymbol{e}) + \boldsymbol{g}_1(\overline{\boldsymbol{x}}+\boldsymbol{e})(\overline{\boldsymbol{u}}+\boldsymbol{u}_{lc}) - \boldsymbol{f}(\overline{\boldsymbol{x}}) - \boldsymbol{g}_1(\overline{\boldsymbol{x}})\overline{\boldsymbol{u}} = \\ \boldsymbol{F}(\overline{\boldsymbol{x}}, \overline{\boldsymbol{u}}, \boldsymbol{e}, \boldsymbol{u}_{lc})\end{gathered} \tag{18}$$

where $\overline{\boldsymbol{x}}$ and $\overline{\boldsymbol{u}}$ can be regarded as time-varying parameters of the system, then (18) changes into

$$\dot{\boldsymbol{e}} = \boldsymbol{F}(\overline{\boldsymbol{x}}, \overline{\boldsymbol{u}}, \boldsymbol{e}, \boldsymbol{u}_{lc}(\boldsymbol{e})) = \boldsymbol{F}(t, \boldsymbol{e}). \tag{19}$$

Linearizing (19) along $(\overline{\boldsymbol{x}}, \overline{\boldsymbol{u}})$ yields

$$\dot{\boldsymbol{e}}(t) = \boldsymbol{A}(t)\boldsymbol{e} + \boldsymbol{B}(t)\boldsymbol{u}_{lc} \tag{20}$$

where $\boldsymbol{A}(t) = [\partial\boldsymbol{f}(\boldsymbol{x})/\partial\boldsymbol{x} + \boldsymbol{u}\cdot\partial\boldsymbol{g}_1(\boldsymbol{x})/\partial\boldsymbol{x}]|_{\overline{\boldsymbol{x}},\overline{\boldsymbol{u}}}, \boldsymbol{B}(t) = \boldsymbol{g}_1(\boldsymbol{x})|_{\overline{\boldsymbol{x}},\overline{\boldsymbol{u}}}$.

Two conclusions can be drawn through (15), (19) and (20).

Conclusion 1 $\boldsymbol{e} = \boldsymbol{0}$ is the isolated equilibrium point; $\boldsymbol{F} : [0,\infty) \times \boldsymbol{D} \to \mathbf{R}^n$ is continuously differentiable, where $\boldsymbol{D} = \{\boldsymbol{e} \in \mathbf{R}^n \|\boldsymbol{e}\| \leqslant r\}$; the Jacobian matrix $[\partial\boldsymbol{F}/\partial\boldsymbol{e}]$ is bounded and Lipschitz on $\boldsymbol{D}$.

Conclusion 2 $\boldsymbol{A}(t)$ and $\boldsymbol{B}(t)$ in (20) are both completely controllable.

For (20), design the state feedback control laws using the PD spectrum [19] of a linear time-varying system as

$$\boldsymbol{u}_{lc} = \boldsymbol{k}(t)\boldsymbol{e}(t). \tag{21}$$

The differential equation of dynamic characteristic of $\boldsymbol{e}$ is

$$\begin{cases}\dot{\boldsymbol{e}}(t) = \boldsymbol{A}_c(t)\boldsymbol{e}(t) \\ \boldsymbol{A}_c(t) = \boldsymbol{A}(t) + \boldsymbol{B}(t)\boldsymbol{k}(t)\end{cases}. \tag{22}$$

Theorem 1 The first equation of (22) is exponentially stable on the equilibrium point $\boldsymbol{e}(t) = \boldsymbol{0}$.

Proof Let

$$\boldsymbol{A}(t) = \frac{\partial\boldsymbol{F}}{\partial\boldsymbol{e}}(t,\boldsymbol{e})\bigg|_{\boldsymbol{e}=\boldsymbol{0}} \tag{23}$$

$$-\dot{\boldsymbol{P}}(t) = \boldsymbol{A}^{\mathrm{T}}(t)\boldsymbol{P}(t) + \boldsymbol{P}(t)\boldsymbol{A}(t) + \boldsymbol{Q}(t). \tag{24}$$

We define $V(t,\boldsymbol{e}) = \boldsymbol{e}^{\mathrm{T}}\boldsymbol{P}(t)\boldsymbol{e}$ as a Lyapunov function candidate for (22). Then

$$\begin{gathered}\dot{V}(t,\boldsymbol{e}) = \boldsymbol{e}^{\mathrm{T}}\boldsymbol{P}(t)\boldsymbol{F}(t,\boldsymbol{e}) + \boldsymbol{F}^{\mathrm{T}}(t,\boldsymbol{e})\boldsymbol{P}(t)\boldsymbol{e} + \boldsymbol{e}^{\mathrm{T}}\dot{\boldsymbol{P}}(t)\boldsymbol{e} = \\ \boldsymbol{e}^{\mathrm{T}}[\boldsymbol{P}(t)\boldsymbol{A}(t) + \boldsymbol{A}^{\mathrm{T}}(t)\boldsymbol{P}(t) + \dot{\boldsymbol{P}}(t)]\boldsymbol{e} + 2\boldsymbol{e}^{\mathrm{T}}\boldsymbol{P}(t)\boldsymbol{G}(t,\boldsymbol{e}) = \\ -\boldsymbol{e}^{\mathrm{T}}\boldsymbol{Q}(t)\boldsymbol{e} + 2\boldsymbol{e}^{\mathrm{T}}\boldsymbol{P}(t)\boldsymbol{G}(t,\boldsymbol{e}) \leqslant \\ -c_3\|\boldsymbol{e}\|^2 + 2c_2L'\|\boldsymbol{e}\|^3 \leqslant \\ -(c_3 - 2c_2L'\rho)\|\boldsymbol{e}\|^2, \quad \forall\|\boldsymbol{e}\|_2 < \rho\end{gathered} \tag{25}$$

where c_2, c_3 are positive constants, L' is a Lipschitz constant, $\boldsymbol{G}(t,\boldsymbol{e}) = \left[\frac{\partial\boldsymbol{F}}{\partial\boldsymbol{e}}(t,\boldsymbol{z}) - \frac{\partial\boldsymbol{F}}{\partial\boldsymbol{e}}(t,\boldsymbol{0})\right]\boldsymbol{e}$, and $\boldsymbol{z}$ is a point on the vector $\boldsymbol{e}$. Choosing $\rho < \min\{r, c_3/(2c_2L)\}$ ensures that $\dot{V}(t,\boldsymbol{e})$ is negatively definited in $\|\boldsymbol{e}\|_2 < \rho$. □

3.2 IGC robustness design by introducing an NDO

In Section 3.1, we suppose that $\boldsymbol{d} = \boldsymbol{0}$, however, it is not the case for practical application. When the error $\|\boldsymbol{d}\|$ is small enough, the tracking error can be bounded or eliminated by designing suitable IGC control laws using TLC. However the effectiveness of the TLC will decrease or even lose completely with the increase of $\|\boldsymbol{d}\|$, so, it is important to take strategies to enhance the robustness.

When $\boldsymbol{d} \neq \boldsymbol{0}$, (19) is given by

$$\dot{\boldsymbol{e}} = \boldsymbol{F}(\overline{\boldsymbol{x}}, \overline{\boldsymbol{u}}, \boldsymbol{e}, \boldsymbol{u}_{lc}) + \boldsymbol{g}_2(\boldsymbol{x})\boldsymbol{d}. \tag{26}$$

Design the strategy as

$$\boldsymbol{u} = \overline{\boldsymbol{u}} + \boldsymbol{u}_{lc} - \boldsymbol{u}_0. \tag{27}$$

According to the NDO output design, define $\boldsymbol{u}_0$ as

$$\boldsymbol{u}_0 = \boldsymbol{g}_0(\boldsymbol{x})\widehat{\boldsymbol{d}} \tag{28}$$

where $\widehat{\boldsymbol{d}} \in \mathbf{R}^3$ is the estimation of $\boldsymbol{d}$.

As $\boldsymbol{g}_1(\boldsymbol{x})\boldsymbol{g}_0(\boldsymbol{x}) = \boldsymbol{g}_2(\boldsymbol{x})$, (26) can be changed into

$$\dot{\boldsymbol{e}} = \boldsymbol{F}(t,\boldsymbol{e}) + \boldsymbol{g}_2(\boldsymbol{x})(\boldsymbol{d} - \widehat{\boldsymbol{d}}). \tag{29}$$

Design the NDO as

$$\begin{cases}\widehat{\boldsymbol{d}} = \boldsymbol{z} + \boldsymbol{p}(\boldsymbol{x}) \\ \dot{\boldsymbol{z}} = -\boldsymbol{l}(\boldsymbol{x})\boldsymbol{g}_2(\boldsymbol{x})[\boldsymbol{z} + \boldsymbol{p}(\boldsymbol{x})] - \boldsymbol{l}(\boldsymbol{x})[\boldsymbol{f}(\boldsymbol{x}) + \boldsymbol{g}_1(\boldsymbol{x})\boldsymbol{u}]\end{cases} \tag{30}$$

where $\boldsymbol{z} \in \mathbf{R}^3$ is the interior state of the NDO, $\boldsymbol{p}(\boldsymbol{x}) \in \mathbf{R}^3$ is a nonlinear function to be set up, $\boldsymbol{l}(x) \in \mathbf{R}^{3\times n}$ denotes the gain of the NDO, with $\boldsymbol{l}(\boldsymbol{x}) = \partial\boldsymbol{p}(\boldsymbol{x})/\partial\boldsymbol{x}$.

The observation error is given as

$$\boldsymbol{e}_{\boldsymbol{d}}(t) = \boldsymbol{d} - \widehat{\boldsymbol{d}}. \tag{31}$$

Let $\dot{\boldsymbol{d}} \approx \boldsymbol{0}$, which means that the unknown disturbance varies slowly with respect to the NDO dynamics. Then, the differential equation of dynamic characteristics of $\boldsymbol{e_d}(t)$ are

$$\dot{\boldsymbol{e}}_{\boldsymbol{d}}(t) = \dot{\boldsymbol{d}} - \dot{\widehat{\boldsymbol{d}}} \approx -\dot{\widehat{\boldsymbol{d}}}. \tag{32}$$

Substituting (14), (30) and (31) into (32), we have

$$\dot{\boldsymbol{e}}_{\boldsymbol{d}}(t) + \boldsymbol{l}(\boldsymbol{x})\boldsymbol{g}_2(\boldsymbol{x})\boldsymbol{e}_{\boldsymbol{d}}(t) = 0. \tag{33}$$

As $\boldsymbol{l}(\boldsymbol{x}) = \partial \boldsymbol{p}(\boldsymbol{x})/\partial \boldsymbol{x}$, $\widehat{\boldsymbol{d}}$ could approximate $\boldsymbol{d}$ exponentially, if $\boldsymbol{e_d}(t)$ is guaranteed to be globally exponentially stable for random $\boldsymbol{x} \in \mathbf{R}^n$ by setting up reasonable $\boldsymbol{p}(\boldsymbol{x})$.

4. Stability analysis of the IGC design method

We give the following lemma to analyze the stability of the IGC design method expediently.

Lemma 1 [20] For an n dimensional linear time-varying system in continuous time:

$$\dot{\boldsymbol{x}} = \boldsymbol{A}(t)\boldsymbol{x}, \quad \boldsymbol{x}(t_0) = \boldsymbol{x}_0 \tag{34}$$

the original point is the sole equilibrium state. Elements in $\boldsymbol{A}(t)$ are all piecewise continuous and uniformly bounded functions. Then, the necessary and sufficient condition for the original point to be exponentially stable is in the following:

For a randomly given real symmetric, uniformly bounded and uniformly positive definited time-varying matrix $\boldsymbol{Q}(t) \in \mathbf{R}^{n\times n}$, there exist two real numbers $\beta_1, \beta_2 > 0$, with $0 < \beta_1\boldsymbol{I} \leqslant \boldsymbol{Q}(t) \leqslant \beta_2\boldsymbol{I}$ $(\forall t \geqslant t_0)$ to make the solution matrix of the differential equation

$$\boldsymbol{A}^{\mathrm{T}}(t)\boldsymbol{P}(t) + \boldsymbol{P}(t)\boldsymbol{A}(t) + \dot{\boldsymbol{P}}(t) + \boldsymbol{Q}(t) = 0 \tag{35}$$

become real symmetric, uniformly bounded and uniformly positive definited, namely that there exist two real numbers $\alpha_1, \alpha_2 > 0$ to satisfy

$$0 < \alpha_1\boldsymbol{I} \leqslant \boldsymbol{P}(t) \leqslant \alpha_2\boldsymbol{I}, \quad t \geqslant t_0. \tag{36}$$

Theorem 2 For the system consisting of (14) and (32), if Conclusions 1 – 2 and the following assumption conditions A1 and A2 are satisfied, we can draw a conclusion that $\boldsymbol{e}$ and $\boldsymbol{e_d}$ are both converged to $\boldsymbol{0}$ exponentially.

A1 For (30), there exists a nonlinear function $\boldsymbol{p}(\boldsymbol{x})$ which makes the error dynamic characteristics of the NDO exponentially stable.

A2 There exist positive real numbers ε and η which satisfy $2\varepsilon - \|\boldsymbol{P}(t)\boldsymbol{g}_2(\boldsymbol{x})\| > 0$, $\eta - 2\ell\alpha_2 r - \|\boldsymbol{P}(t)\boldsymbol{g}_2(\boldsymbol{x})\| > 0$, with ℓ being a Lipschitz constant.

Proof From Conclusions 1 – 2, by using the Taylor expansion, (29) can be expressed as

$$\dot{\boldsymbol{e}} = \boldsymbol{A}(t)\boldsymbol{e}(t) + \boldsymbol{B}(t)\boldsymbol{u} + \boldsymbol{0}(\bullet) + \boldsymbol{g}_2(\boldsymbol{x})(\boldsymbol{d} - \widehat{\boldsymbol{d}}) \tag{37}$$

where $\boldsymbol{0}(\bullet)$ stands for the linear high order term.

From the proof process of Theorem 1, we have

$$\|\boldsymbol{0}(\bullet)\| \leqslant \ell\|\boldsymbol{e}(t)\|^2. \tag{38}$$

From A1, there exists a Lyapunov function $V_d(e_d)$ for (32), which satisfies

$$\dot{V}_d = -\frac{\partial V_d}{\partial e_d^i}\left[\frac{\partial p^i(\boldsymbol{x})}{\partial \boldsymbol{x}}\boldsymbol{g}_2^i(\boldsymbol{x})e_d^i\right] \leqslant -\gamma\|e_d^i\|^2, \quad i = 1, 2, 3 \tag{39}$$

where e_d^i is the ith element of $\boldsymbol{e_d}(t)$, $p^i(\boldsymbol{x})$ is the ith element of $\boldsymbol{p}(\boldsymbol{x})$, and $\boldsymbol{g}_2^i(\boldsymbol{x})$ is the ith element of $\boldsymbol{g}_2(\boldsymbol{x})$.

For the whole closed-loop system, consider the Lyapunov function

$$V = \frac{1}{2}\boldsymbol{e}^{\mathrm{T}}\boldsymbol{P}(t)\boldsymbol{e} + V_d(e_d^i). \tag{40}$$

Taking the derivative of both sides of (40) with respect to time, according to Lemma 1, (38) and (39), we have

$$\begin{aligned}\dot{V} = &-\frac{1}{2}\boldsymbol{e}^{\mathrm{T}}\boldsymbol{Q}(t)\boldsymbol{e} + \boldsymbol{e}^{\mathrm{T}}\boldsymbol{P}(t)0(\bullet) + \boldsymbol{e}^{\mathrm{T}}\boldsymbol{P}(t)\boldsymbol{g}_2(\boldsymbol{x})e_d^i + \dot{V}_d \leqslant \\ &-\frac{1}{2}\eta\|\boldsymbol{e}\|^2 + \alpha_2\ell\|\boldsymbol{e}\|^3 + \|\boldsymbol{P}(t)\boldsymbol{g}_2(\boldsymbol{x})\|\|\boldsymbol{e}\|\|e_d^i\| - \varepsilon\|e_d^i\|^2 \leqslant \\ &-\frac{1}{2}(\beta_1 - 2\alpha_2\ell R_e - \|\boldsymbol{P}(t)\boldsymbol{g}_2(\boldsymbol{x})\|)\|\boldsymbol{e}\|^2 - \\ &\frac{1}{2}(2\varepsilon - \|\boldsymbol{P}(t)\boldsymbol{g}_2(\boldsymbol{x})\|)\|e_d^i\|.\end{aligned} \tag{41}$$

From A2, one can obtain $\dot{V} < 0$. □

The stability of the proposed IGC design method can be guaranteed by selecting reasonable $\boldsymbol{p}(\boldsymbol{x})$ and appropriate values of ε and η.

5. Simulation and results discussion

In order to validate the effectiveness of the proposed IGC design method in this paper, we simulate a terminal attack mission of the suicide UCAV with six-degree-of-freedom nonlinear experiments.

In the initial time, the suicide UCAV is trimmed under the cruise conditions before attacking the target: $V_0 = 200$ m/s, $\delta_z = 5°$, $\alpha_0 = \theta_0 = 1.328\,9°$, with the initial coordinate $[500\ \mathrm{m}, 3\,000\ \mathrm{m}, 500\ \mathrm{m}]^{\mathrm{T}}$.

The gain matrix $\boldsymbol{k}(t)$ and nonlinear function $\boldsymbol{p}(\boldsymbol{x})$ of the proposed method are set as

$$\boldsymbol{k}(t) = [\boldsymbol{k}_1(t)\ \boldsymbol{k}_2(t)\ \boldsymbol{k}_3(t)]$$

$$\boldsymbol{k}_1(t) = [2.5t^2 + 3\ \ 1.5t + 6\ \ 0.5t^2 + 8t - 4.8]$$

$$\boldsymbol{k}_2(t) = [1.4t^2 + 5\ \ 0.6t + 8\ \ 1.2t^2 + 5t - 3.6]$$

$$\boldsymbol{k}_3(t) = [2.2t + 3\ \ 0.8t^2 + 3t - 5.0]$$

$$\boldsymbol{p}(\boldsymbol{x}) = [p_1(\boldsymbol{x}_1)\ p_2(\boldsymbol{x}_2)\ p_3(\boldsymbol{x}_3)]^{\mathrm{T}}$$

$$p_1(\boldsymbol{x}_1) = \dot{\varphi}_{ry}^2 + 3\dot{\varphi}_{ry}\alpha - 2\alpha\omega_z - \alpha^2 + 4\omega_z^2$$

$$p_2(\boldsymbol{x}_2) = \dot{\varphi}_{rz}^2 + 3\dot{\varphi}_{rz}\beta - 2\beta\omega_y - \beta^2 + 4\omega_y^2$$

$$p_3(\boldsymbol{x}_3) = -2\gamma\omega_x - \gamma^2 + 4\omega_x^2.$$

Parameters of the pseudo differentiator are given by $\omega_{1,diff} = 3.5\ \mathrm{rad/s}$, $\omega_{2,diff} = 8\ \mathrm{rad/s}$.

The initial position, velocity and acceleration vectors of the target are, respectively, set as

$$\begin{cases} \boldsymbol{X}_t = [0\ 0\ 300\ \mathrm{m}]^{\mathrm{T}} \\ \boldsymbol{V}_t = [40\ \mathrm{m/s}\ 0\ 10\ \mathrm{m/s}]^{\mathrm{T}} \\ \boldsymbol{a}_t = [5\ \mathrm{m/s^2}\ 0\ 1\ \mathrm{m/s^2}]^{\mathrm{T}} \end{cases}.$$

First of all, we make a comparison of control performance of our proposed method in this paper, the traditional method [21] and the VSC method [22], in the presence of 20% aerodynamic coefficients uncertainty and 20% noise interference in measure values. Three independent experiments are simulated based on the above methods, and the suicide UCAV intercepts the target, respectively, at 22.89 s, 23.40 s, and 24.12 s under three cases. Miss distance comparison with the proposed method, traditional method and VSC method is shown in Table 1. Curves of the angles, curves of the derivatives, curves of the fin deflection, and trajectories of the suicide UCAV and target are, respectively, shown in Figs. 3 – 6.

As is shown in Table 1 and Figs. 3 – 6, we see that the miss distance of the proposed method is the least. Although the VSC method has little miss distance too, big oscillation occurs in the simulation process, which means that the dynamic performance of the VSC method is not good. Small oscillation can be guaranteed for the traditional method, but the convergence time is too long, besides, the miss distance is up to 6.263 3 m, which illustrates that the control accuracy of the traditional method is low.

Table 1 Miss distance comparison with the proposed method, traditional method and VSC method

Method	Miss distance/m
Proposed method	0.038 5
Traditional method	6.263 3
VSC method	0.797 5

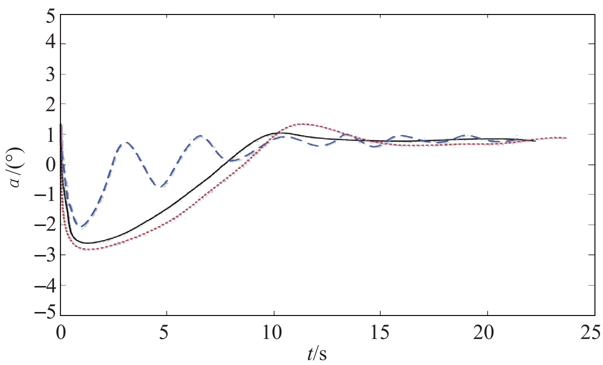

(a) α

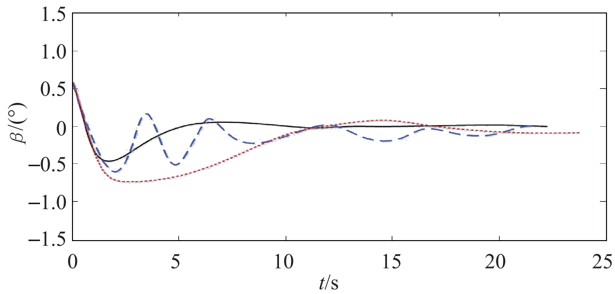

(b) β

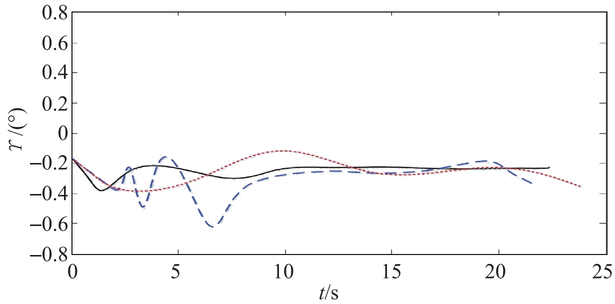

(c) γ

: Proposed method; : VSC method;
: Traditional method.

Fig. 3 Curves of the angles α, β and γ

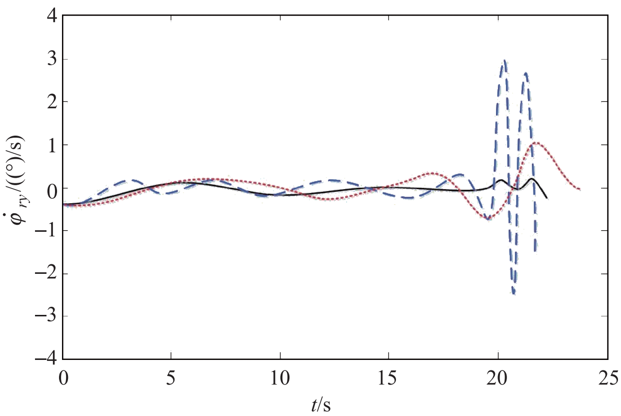

(a) $\dot{\varphi}_{ry}$

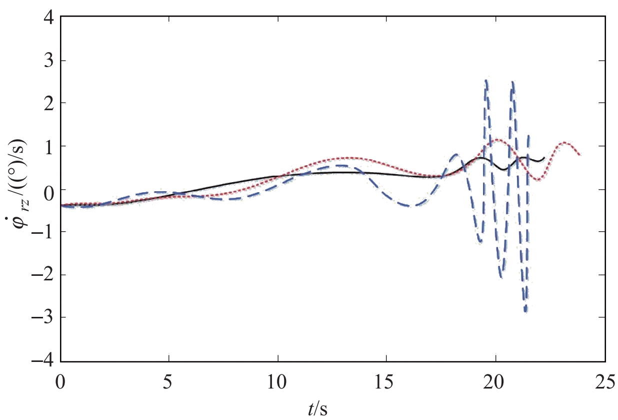

(b) $\dot{\varphi}_{rz}$

: Proposed method; : VSC method;
: Traditional method.

Fig. 4 Curves of the derivatives of φ_{ry} and φ_{rz}

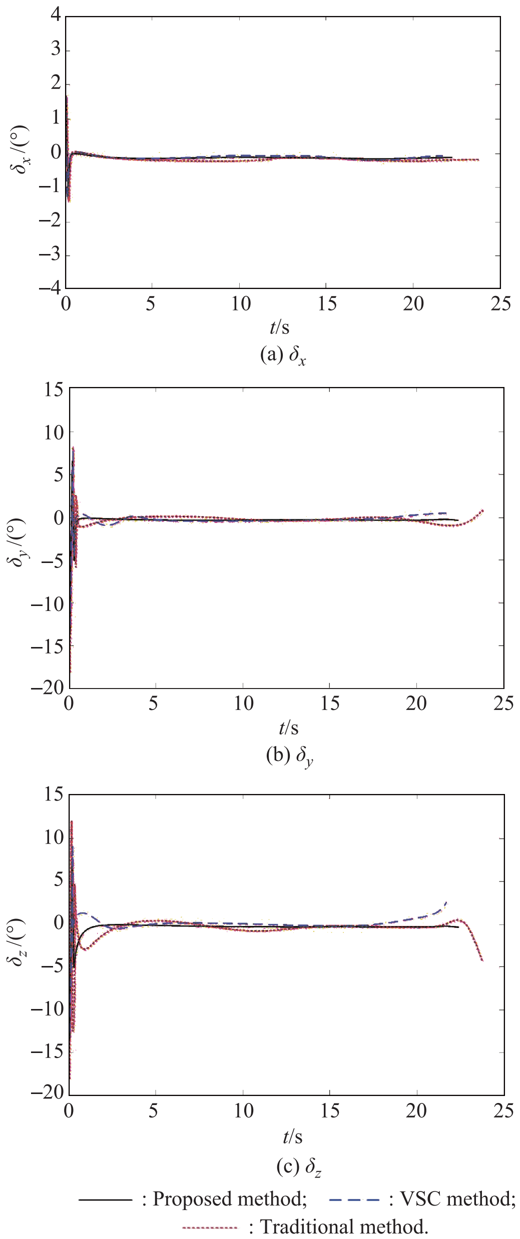

Fig. 5 Curves of the fin deflection δ_x, δ_y and δ_z

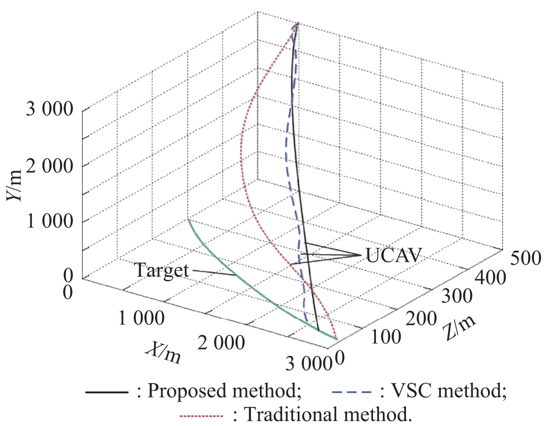

Fig. 6 Trajectories of the suicide UCAV and target

To summarize, the proposed method can guarantee not only high-precision control performance but also good dynamic response behavior.

We further test the robustness of the proposed IGC design method against time-varying uncertainty. Let aerodynamic coefficients uncertainty and noise interference in measure values both subject to the following distribution:

$$\Delta \sim U(-0.2,\ 0.2)$$

where U represents the uniform distribution.

We repeat the robustness experiment 50 times using the Monte Carlo method [23] and the results are depicted in Fig. 7. Through the statistical analysis, we know that the mean miss distance is 0.039 6 m with the standard deviation being 0.018 9 m, which conforms to the control performance experiment results. While the aerodynamic coefficients uncertainty and noise interference vary randomly within $[-20\%, 20\%]$, the UCAV's angle of attack, sideslip, and roll are, respectively, converged within $[-1°, 1°]$, $[-0.5°, 0.5°]$ and $[-0.1°, 0.1°]$. The angle of roll changes within $[-0.2°, 0.2°]$ throughout the engagement. All the states meet the design objectives of the suicide UCAV control system, which validates the strong robustness of the proposed method.

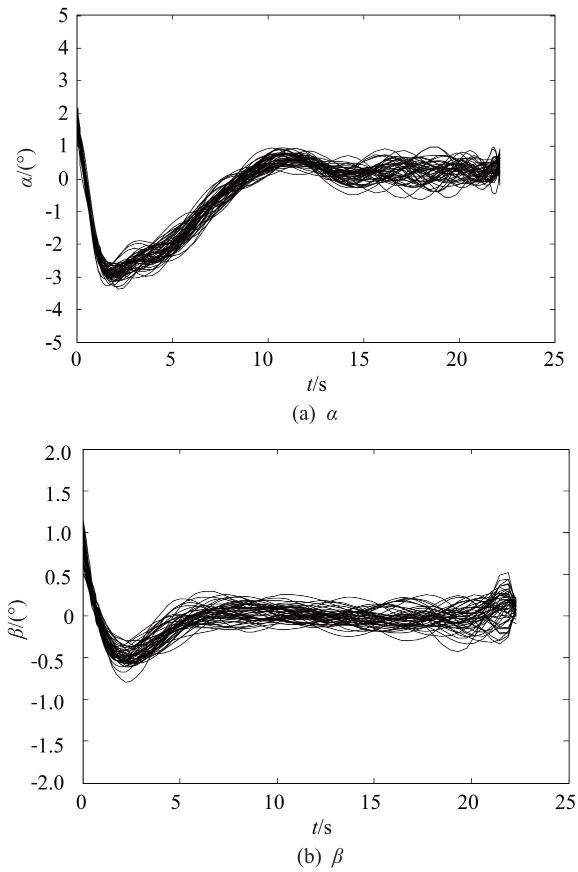

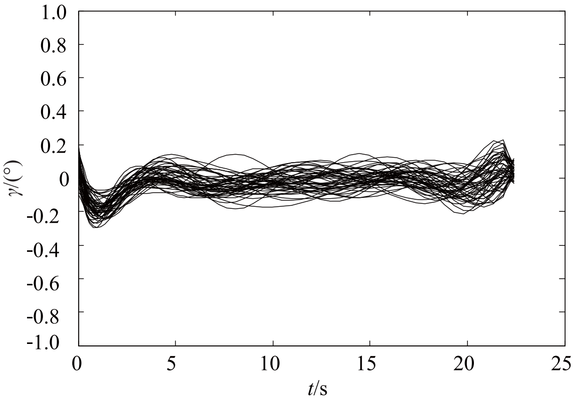

(c) γ

Fig. 7 Curves of the angles α, β and γ in the presence of time-varying model uncertainty

6. Conclusions

The IGC system model of the suicide UCAV in terminal attack phase is built, and the difficulties of designing the controller are reduced greatly. IGC control laws are designed by using TLC. The design method can guarantee strong robustness by introducing an NDO. Lyapunov-based analysis shows that the proposed control strategy can completely eliminate the tracking errors in the presence of constant or time-varying uncertainties. The performance of the proposed IGC design method is evaluated in a terminal attack mission of the suicide UCAV. Simulation results show that the novel method can control the UCAV states well even in the presence of 20% model uncertainty of both constant and time-varying types. The research results will benefit practical missions of suicide UCAVs in the future.

References

[1] W. R. Zhu, H. B. Duan. Chaotic predator-prey biogeography-based optimization approach for UCAV path planning. *Aerospace Science and Technology*, 2014, 32(1): 153 – 161.

[2] L. Maital, S. Tal, G. Shual. Linear quadratic integrated vs separated autopilot-guidance design. *Journal of Guidance, Control, and Dynamics*, 2013, 36(6): 1722 – 1730.

[3] W. R. Yueh, C. F. Lin. Optimal controller for homing missile. *Proc. of the American Control Conference*, 1984: 737 – 742.

[4] B. Yang, G. A. Liang, J. H. Peng. Self-adaptive PID controller of microwave drying rotary device tuning on-line by genetic algorithms. *Journal of Central South University*, 2013, (20): 2685 – 2692.

[5] Y. Zhang, J. Chen, L. C. Shen. Real-time trajectory planning for UCAV air-to-surface attack using inverse dynamics optimization method and receding horizon control. *Chinese Journal of Aeronautics*, 2013, 26(4): 1038 – 1056.

[6] M. Z. Hou, X. L. Liang, G. R. Duan. Adaptive block dynamic surface control for integrated missile guidance and autopilot. *Chinese Journal of Aeronautics*, 2013, 26(3): 741 – 750.

[7] D. E. Williams, J. Richman, B. Friedland. Design of an integrated strap down guidance and control system for a tactical missile. *Proc. of the Guidance and Control Conference*, 1983: 57 – 66.

[8] C. F. Lin, E. Ohlmeyer, J. E. Bibel, et al. Optimal design of integrated missile guidance and control. *Proc. of the World Aviation Conference*, 1998: 1 – 13.

[9] M. Sharma, N. D. Richards. Adaptive integrated guidance and control for missile interceptors. *Proc. of the AIAA Guidance, Navigation, and Control Conference*, 2004: 1 – 15.

[10] X. L. Shao, H. L. Wang. Back-stepping active disturbance rejection control design for integrated missile guidance and control system via reduced-order ESO. *ISA Transaction*, 2015, 57: 10 – 22.

[11] P. K. Menon, E. J. Ohlmeyer. Nonlinear integrated guidance-control laws for homing missiles. *Proc. of the AIAA Guidance, Navigation, and Control Conference*, 2001: 1 – 9.

[12] X. F. Wang, Y. Y. Zheng, H. Lin. Integrated guidance and control law for cooperative attack of multiple missiles. *Aerospace Science and Technology*, 2015, 42: 1 – 11.

[13] T. Shima, M. Idan, O. M. Golan. Sliding mode control for integrated missile autopilot-guidance. *Journal of Guidance, Control and Dynamics*, 2006, 29(2): 250 – 260.

[14] J. J. Zhu, A. Huizenga. A type two trajectory linearization controller for a reusable launch vehicles a singular perturbation approach. *Proc. of the AIAA Atmospheric Flight Mechanics Conference*, 2004: 1 – 16.

[15] Y. Liu, R. Huang, J. Zhu. Adaptive neural network control based on trajectory linearization control. *Proc. of the 6th World Congress on Intelligent Control and Automation*, 2006: 417 – 421.

[16] Z. P. Jiang. Global tracking control of underactuated ships by Lyapunov's direct method. *Automatica*, 2002, 38(2): 301 – 309.

[17] H. Zhou, H. Q. Huang, T. Han, et al. Robust integrated guidance and control design method for UCAV based on trajectory linearization control. *Proc. of the 15th International Conference on Control, Automation and Systems*, 2015: 1030 – 1035.

[18] M. Z. Hou, G. R. Duan. Robust adaptive dynamic surface control of uncertain nonlinear systems. *International Journal of Control Automatic System*, 2011, 9(1): 161 – 168.

[19] M. C. Mickle, J. J. Zhu. Bank-to-turn roll-yaw-pitch auto-pilot design using dynamic nonlinear inversion and PD-eigenvalue assignment. *Proc. of the American Control Conference*, 2000: 1359 – 1364.

[20] H. K. Kahlil. *Nonlinear systems*. New Jersey, USA: Prentice-Hall, 2002.

[21] B. Yang, G. A. Liang, J. H. Peng. Self-adaptive PID controller of microwave drying rotary device tuning on-line by genetic algorithms. *Journal of Central South University*, 2013, (20): 2685 – 2692.

[22] I. Nagesh, C. Edwards. A multivariable super-twisting sliding mode approach. *Automatica*, 2014, 50(3): 984 – 988.

[23] R. Liu, X. X. Sun, W. H. Dong. Dynamics modeling and control of a transport aircraft for ultra-low altitude airdrop. *Chinese Journal of Aeronautics*, 2015, 28(2): 478 – 487.

Biographies

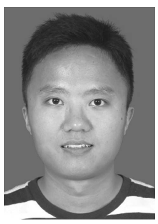

Huan Zhou was born in 1989. He received his M.S. degree in fight system and technology of UAV from Air Force Engineering University in 2011. He is now a Ph.D. degree candidate in Air Force Engineering University. His research interests are navigation, guidance and control of UAV and cooperative control of aircrafts.
E-mail: zd578500633@126.com

Hui Zhao was born in 1973. He received his Ph.D. degree in weapon science and technology from Air Force Engineering University in 2011. He is currently a professor in Aeronautics and Astronautics Engineering College, Air Force Engineering University. He has been engaged in teaching and researching on weapon systems and application engineering and optimal control.
E-mail: zhaohui_kgy@163.com

Hanqiao Huang was born in 1982. He received his Ph.D. degree in navigation, guidance and control from Northwestern Polytechnical University in 2010. He is currently an instructor and working in Aeronautics and Astronautics Engineering College, Air Force Engineering University. His research interests are optimal control and control science and engineering.
E-mail: cnaxhhq@126.com

Xin Zhao was born in 1982. He received his Ph.D. degree in aviation detection technology from Air Force Engineering University in 2010. He is currently an instructor and working in Aeronautics and Astronautics Engineering College, Air Force Engineering University. His research interests are detection technology and fault-tolerant control.
E-mail: kgy_zhaox@163.com